Remote sensing studies of the Dionysius region of the Moon

T. A. Giguere,[1,2] B. Ray Hawke,[1] L. R. Gaddis,[3] D. T. Blewett,[4] J. J. Gillis-Davis,[1] P. G. Lucey,[1] G. A. Smith,[1] P. D. Spudis,[5] and G. J. Taylor[1]

Received 15 November 2005; revised 25 January 2006; accepted 27 February 2006; published 17 June 2006.

[1] The Dionysius region is located near the western edge of Mare Tranquillitatis and is centered on Dionysius crater, which exhibits a well-developed dark ray system. Proposed origins for these dark rays included impact melt deposits and dark primary ejecta. The region also contains extensive deposits of Cayley-type light plains. Clementine multispectral images and a variety of spacecraft photography were utilized to investigate the composition and origin of geologic units in the Dionysius region. The portions of the dark rays for which spectral and chemical data were obtained are composed of mare debris contaminated with minor amounts of highland material. Both five-point spectra and values of the optical maturity (OMAT) parameter indicate that the dark rays are dominated by mare basalts, not glassy impact melts. The high-albedo rays associated with Dionysius exhibit FeO and TiO_2 values that are lower than those of the adjacent dark ray surfaces and OMAT values that indicate that bright ray surfaces are not fully mature. The high-albedo rays are bright largely because of the contrast in albedo between ray material containing highlands-rich ejecta and the adjacent mare-rich surfaces. The mafic debris ejected by Dionysius was derived from a dark, iron-rich unit exposed high on the inner wall of the crater. This layer probably represents a mare deposit that was present at the surface of the preimpact target site. With one possible exception, there is no evidence for buried mare basalts associated with Cayley plains in the region.

Citation: Giguere, T. A., B. R. Hawke, L. R. Gaddis, D. T. Blewett, J. J. Gillis-Davis, P. G. Lucey, G. A. Smith, P. D. Spudis, and G. J. Taylor (2006), Remote sensing studies of the Dionysius region of the Moon, *J. Geophys. Res.*, *111*, E06009, doi:10.1029/2005JE002639.

1. Introduction and Background

[2] The Dionysius region (Figure 1) is located near the western edge of Mare Tranquillitatis and is centered on Dionysius crater (2.8°N, 17.3°E). The region contains a portion of Mare Tranquillitatis, highland terrain, extensive deposits of Cayley-type light plains, and Rima Ariadaeus (Figures 2 and 3). The region also contains the type area of the Cayley Formation [*Morris and Wilhelms*, 1967].

[3] Dionysius is an 18 km diameter crater that exhibits a well-developed dark ray system (Figure 3). The nature and origin of this Copernican-aged crater and its dark rays have long been the subject of much controversy. The results of a detailed photographic study of Dionysius crater were presented by *Smalley* [1965]. He noted that rather than having bright rays similar to those of Copernicus, Kepler, and other young craters, Dionysius displays rays of dark material. *Smalley* [1965] determined that the dark rays of Dionysius are symmetrical about the crater and that several of its rays extend out over the mare and that those that do are darker than the mare surface. He concluded that there was insufficient evidence to determine the origin of Dionysius and that both volcanism and impact were viable hypotheses for the origin of the dark rays. More recently, *Morris and Wilhelms* [1967] and *Schultz* [1976] used morphologic evidence to demonstrate the impact origin of Dionysius crater. Still, the nature and origin of the dark rays remain uncertain. Proposed origins include low-albedo impact melt deposits and dark primary ejecta from Dionysius [e.g., *Morris and Wilhelms*, 1967; *Schultz*, 1976; *Schultz and Spudis*, 1979; *Hawke et al.*, 1979]. It has been proposed that the dark primary ejecta was derived from surface basalt flows [*Thomson et al.*, 1998; *Li and Mustard*, 2000a], buried mare basalts (i.e., cryptomare) [*Schultz and Spudis*, 1979; *Staid et al.*, 1996], or a mafic plutonic complex [*Schultz and Spudis*, 1979].

[4] The Dionysius region contains major expanses of light plains deposits that were mapped as the Cayley Formation by *Morris and Wilhelms* [1967]. The type area for the Cayley Formation is located just east of Cayley crater (Figures 2 and 3). The surface of the Cayley Formation is flat and smooth and exhibits a higher albedo and crater density than the basalt flows in Mare Tranquillitatis [*Morris and Wilhelms*, 1967]. Cryptomare deposits are associated with Cayley-type light plains in some portions

[1]Hawaii Institute of Geophysics and Planetology, University of Hawaii at Manoa, Honolulu, Hawaii, USA.
[2]Also at Intergraph Corporation, Honolulu, Hawaii, USA.
[3]U.S. Geological Survey, Flagstaff, Arizona, USA.
[4]NovaSol, Honolulu, Hawaii, USA.
[5]Johns Hopkins University Applied Physics Laboratory, Laurel, Maryland, USA.

0148-0227/06/2005JE002639$09.00

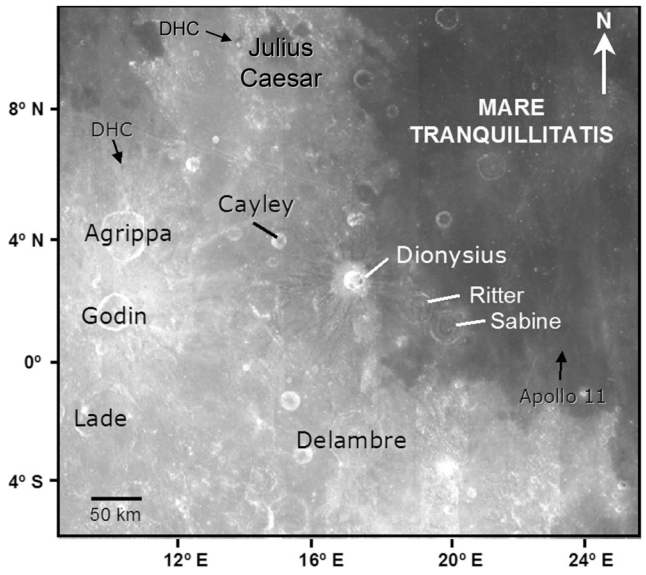

Figure 1. Clementine 750 nm image mosaic showing the portion of the lunar nearside that contains the Dionysius region under high Sun illumination. The image mosaic has a spatial resolution of 1 km/pixel. DHCs indicate dark-haloed impact craters.

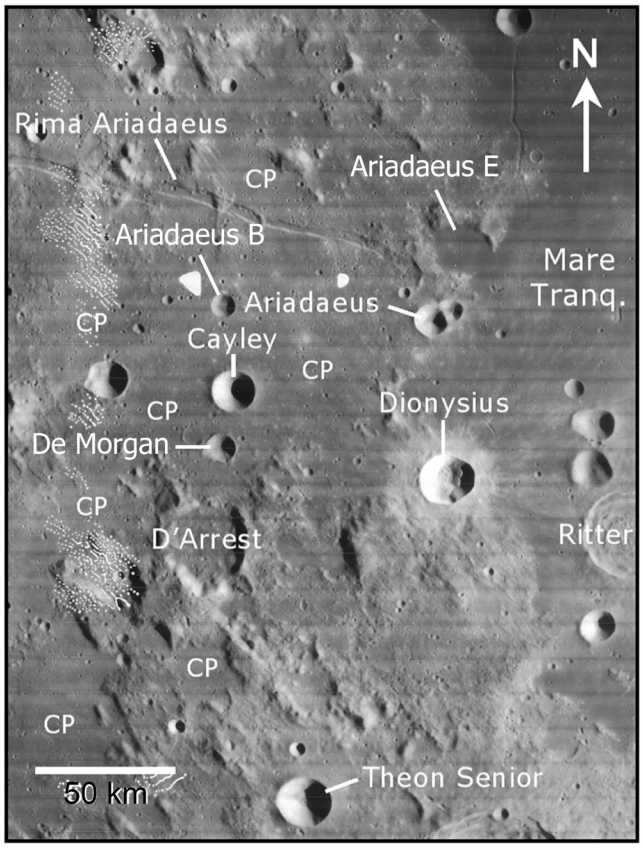

Figure 2. Portion of Lunar Orbiter IV frame 90-H1 showing the morphologies of features in the Dionysius region. CPs indicate the locations of Cayley plains units.

of the lunar surface [e.g., *Hawke and Spudis*, 1980; *Hawke et al.*, 1985; *Antonenko et al.*, 1995]. The existence of flat expanses of mare terrain should facilitate the formation of light plains deposits by debris surges produced by the impact of secondary-forming projectiles ejected by large basin-forming impacts [*Hawke and Bell*, 1981; *Bell and Hawke*, 1984; *Blewett et al.*, 1995; *Giguere et al.*, 2003]. This is because level mare surfaces allow debris surges from large impacts to travel unimpeded across flat topography. *Staid et al.* [1996] presented several lines of evidence that suggest that the Cayley Formation along the western Tranquillitatis margin may lie on top of an ancient mare deposit buried by Imbrium basin ejecta (i.e., a cryptomare deposit).

[5] Clementine multispectral images and a variety of spacecraft photography were utilized to investigate the composition and origin of geologic units in the Dionysius region. The goals of this study include the following: (1) to determine the composition and origin of the dark and bright rays associated with Dionysius, (2) to investigate the origin of mafic material exposed by Dionysius crater, and (3) to identify possible cryptomare deposits in the region.

2. Data and Methods

[6] A variety of spacecraft imagery was used to study the Dionysius region. These included Lunar Orbiter and Apollo photographs. The primary data used for this investigation were images obtained by the Clementine UV-VIS camera. While the Clementine images provide high spatial resolution (~100–200 m/pixel), they are of low spectral resolu-

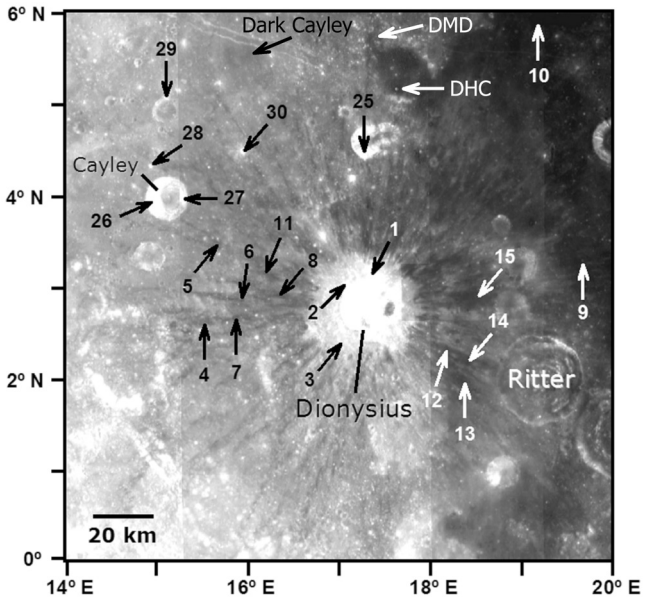

Figure 3. Clementine 750 nm image mosaic of the Dionysius region. The image mosaic has a spatial resolution of 190 m/pixel. The numbered arrows show the locations where the five-point spectra shown in Figures 5 and 6 were obtained (see Table 2). DHC indicates the location of a dark-haloed impact crater. A previously unidentified dark mantle deposit of probable pyroclastic origin is labeled DMD. Dark Cayley refers to an area of the Cayley Formation with a relatively low albedo.

tion. However, the band passes of the UV-VIS camera filters (415, 750, 900, 950, and 1000 nm) were chosen specifically for lunar investigation by the Clementine science team to maximize the information content returned by this multispectral instrument [*Nozette et al.*, 1994].

[7] The U.S. Geological Survey's Astrogeology Program has published on CD-ROM a Clementine five-color UV-VIS digital image model (DIM) for the Moon [*Robinson et al.*, 1999; *Eliason et al.*, 1999; *Isbell et al.*, 1999]. UV-VIS data from this DIM were used to produce an image cube centered on the Dionysius region with a spatial resolution of 190 m/pixel (Figure 3). This image cube, calibrated to reflectance, served as the basis for the production of a number of data products, including FeO and TiO_2 maps.

[8] The FeO map shown in Figure 4a was prepared using the algorithms of *Lucey et al.* [2000a]. The technique developed by *Lucey et al.* [1995] for determining FeO abundances uses 750 nm reflectance and 950 nm/750 nm ratio images to measure the spectral effects of ferrous iron in major lunar minerals such as olivine and pyroxene. This method controls for the optical effects of the submicroscopic metallic iron that is produced as rocks and soils are exposed to micrometeorite bombardment and solar wind implantation at the lunar surface [*Lucey et al.*, 1995; *Hapke*, 2001]. The TiO_2 map of the Dionysius region (Figure 4b) was produced using the technique described by *Lucey et al.* [1998, 2000a]. This method utilizes a spectral parameter derived from 750 nm reflectance and 415 nm/750 nm ratio images. The mapping from the color-albedo parameter to wt % TiO_2 is based on an understanding of the spectral effects of the Ti-rich opaque mineral ilmenite ($FeTiO_3$) as a component of a mineral mixture comprising the lunar regolith at the locations sampled by Apollo and Luna [*Blewett et al.*, 1997; *Lucey et al.*, 1998, 2000a; *Jolliff*, 1999; *Blewett and Hawke*, 2001]. An optical maturity (OMAT) image (Figure 7c) was produced for the Dionysius region using the algorithms of *Lucey et al.* [2000b]. OMAT parameter data are useful for investigating the relative maturity of surface units.

[9] The average FeO, TiO_2, and OMAT values for selected areas in the Dionysius region are listed in Table 1. These areas include dark and bright rays, high-albedo ejecta, and mare surfaces. The locations of the areas for which the averages were obtained are indicated by black boxes in Figure 4a. Generally, the values were obtained by averaging a 3×3 pixel matrix in the area of interest. However, some averages were made for larger areas (A, B, G, O, P, Q, and S in Figure 4a). Care was taken to avoid steep slopes because of topographic effects that may affect FeO, TiO_2, and OMAT estimates [e.g., *Jolliff*, 1999].

[10] Recent efforts have demonstrated that Clementine five-point spectra can be used to derive a number of diagnostic parameters that can be utilized to determine the lithology of the areas for which the spectra were obtained [*Tompkins and Pieters*, 1999; *Pieters et al.*, 2001]. We have used five-point spectra extracted from the registered and calibrated Clementine UV-VIS images to investigate the composition of surface units in the Dionysius region (Figures 5 and 6). The techniques described by *Tompkins and Pieters* [1999] and *Pieters et al.* [2001] were employed. The spectra shown in Figures 5 and 6 are the average of nine pixels. The locations for which these spectra were obtained are indicated by black arrows in Figures 3 and 7b and described in Table 2.

3. Results and Discussion

3.1. Dionysius Crater Rays

3.1.1. Dark Rays

[11] Well-developed dark rays were mapped in the highlands west of Dionysius crater by *Morris and Wilhelms* [1967] (Figures 1 and 3). FeO and TiO_2 maps produced from Clementine UV-VIS images were used to determine the compositions of the darkest portions of the rays (Figure 4 and Table 1). The average FeO and TiO_2 values range between 13.2 wt % and 15.6 wt % FeO and from 3.7 wt % to 5.8 wt % TiO_2. In contrast, the high-albedo proximal ejecta immediately west of Dionysius (Area B in Figure 4a and Table 1) exhibits FeO values of $\sim$9 wt % and TiO_2 values of $\sim$2 wt %. Even lower FeO and TiO_2 concentrations are exhibited by the bright ejecta immediately north of Dionysius (Area A in Figure 4a and Table 1). The background highlands terrain west of Dionysius crater generally has FeO abundances $<$10 wt % and TiO_2 abundances $<$2.5 wt %. Much higher FeO and TiO_2 values are associated with the mare basalt flows in Mare Tranquillitatis (Areas O and P in Figure 4a and Table 1). The high FeO and TiO_2 values exhibited by the dark rays west of Dionysius suggest that they contain large amounts of mare material.

[12] In order to further investigate the mineralogy and lithology of the dark rays, five- point spectra were acquired for the dark rays and bright proximal ejecta north and west of the crater as well as impact craters and mature surfaces in Mare Tranquillitatis (Figures 5 and 6a). The areas for which these spectra were obtained are shown in Figure 3 and described in Table 2. The three representative spectra extracted for the high-albedo proximal ejecta (1, 2, and 3 in Figure 5a) exhibit high reflectance values and have absorption bands centered near 0.90 μm, which suggests a mafic assemblage dominated by low-Ca pyroxene. The band centers and shapes indicate that these ejecta deposits are composed largely of anorthositic norites. The spectra obtained for relatively young impact craters in Mare Tranquillitatis (e.g., 9 in Figure 5a and 21 and 24 in Figure 6a) exhibit "1 μm" absorption features, and the band shapes indicate mafic assemblages dominated by high-Ca clinopyroxene. Spectra were extracted for six dark ray segments west of Dionysius (4–8 in Figure 5a and 11 in Figure 5b). These spectra have "1 μm" absorption bands that are centered near 0.95 μm, which indicate the dominance of high-Ca pyroxene. The dark ray spectra are very similar to the spectra collected for mare craters in Mare Tranquillitatis. However, the dark ray spectra exhibit slightly higher reflectance values than those of the mare craters. The portions of the dark rays for which the spectra were obtained are composed of mare debris contaminated with lesser amounts of highland material.

[13] Fully mature surfaces in the Dionysius region exhibit OMAT values that range between 0.116 and 0.123. In contrast, an extremely young, small impact crater northeast of Cayley crater (R in Figure 4a and Figure 8) has an OMAT value of 0.329. The OMAT values of high-albedo proximal ejecta north and west of Dionysius range from 0.163 to 0.168 (areas A and B in Figure 4a and Table 1). While the

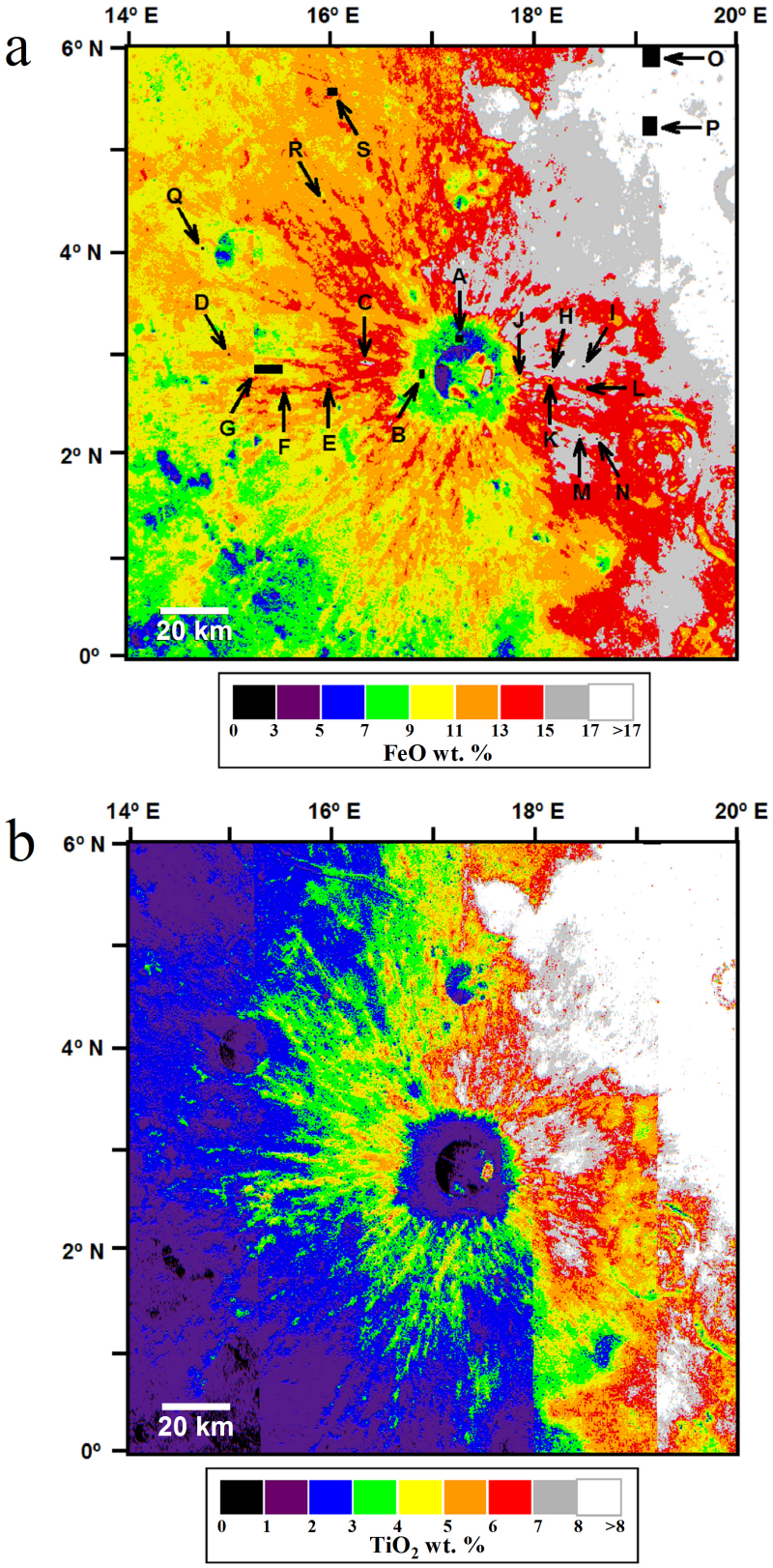

Figure 4. (a) FeO map derived from Clementine UV-VIS images for the Dionysius region. This image, as well as the TiO_2 map shown in Figure 4b, covers the area shown in Figure 3. The black boxes indicate the areas for which the average FeO, TiO_2, and OMAT values were obtained. These areas are identified with letters, and the average values are listed in Table 1. (b) TiO_2 map of the Dionysius region.

Table 1. Average FeO, TiO_2, and OMAT Values for Selected Areas in the Dionysius Region[a]

Area	Description	FeO, wt %	TiO_2, wt %	OMAT Parameter
A	north ejecta	6.9 ± 0.9	1.6 ± 0.3	0.168 ± 0.017
B	west ejecta	9.1 ± 0.4	1.9 ± 0.3	0.163 ± 0.006
C	west dark ray (proximal)	15.6 ± 0.2	5.8 ± 0.2	0.149 ± 0.004
D	west dark ray (distal)	13.2 ± 0.3	3.7 ± 0.1	0.149 ± 0.005
E	SW dark ray (proximal)	14.4 ± 0.3	4.9 ± 0.4	0.144 ± 0.008
F	SW dark ray (distal)	14.1 ± 0.2	4.7 ± 0.3	0.144 ± 0.005
G	west interray area	9.6 ± 0.5	2.4 ± 0.2	0.128 ± 0.009
H	east dark ray (proximal)	16.0 ± 0.1	8.0 ± 0.2	0.144 ± 0.004
I	east dark ray (distal)	16.5 ± 0.0	8.0 ± 0.2	0.141 ± 0.002
J	east bright ray (proximal)	10.3 ± 0.2	3.4 ± 0.2	0.134 ± 0.004
K	east bright ray	12.5 ± 0.2	5.5 ± 0.3	0.134 ± 0.003
L	east bright ray (distal)	12.8 ± 0.2	5.5 ± 0.1	0.135 ± 0.005
M	SE dark ray (proximal)	15.8 ± 0.1	7.0 ± 0.3	0.137 ± 0.006
N	SE dark ray (distal)	16.0 ± 0.1	7.4 ± 0.3	0.146 ± 0.004
O	mare surface (North)	18.1 ± 0.3	10.9 ± 0.9	0.116 ± 0.007
P	mare surface (South)	17.6 ± 0.2	9.8 ± 0.4	0.119 ± 0.007
Q	Cayley plains	9.4 ± 0.3	1.9 ± 0.1	0.122 ± 0.005
R	small crater	13.4 ± 0.2	1.6 ± 0.1	0.329 ± 0.006
S	dark Cayley plains	13.2 ± 0.2	3.4 ± 0.2	0.125 ± 0.005

[a]The areas for which the averages were obtained are shown in Figure 4a. The listed uncertainties are one standard deviation.

darkest portions of the rays west of Dionysius exhibit lower OMAT values (0.144–0.149, Table 1), they are not fully mature. It has been noted that impact melts around very young craters will appear relatively mature in optical maturity images [e.g., *Lucey et al.*, 2000b; *Hawke et al.*, 2002]. Both the five-point spectra discussed above and the OMAT values indicate that the dark rays are dominated by mare basalt, not impact melt.

[14] As noted by *Smalley* [1965], the dark rays west of Dionysius generally become brighter at greater distances from the crater until they finally disappear (Figures 1 and 3). The FeO and TiO_2 images (Figure 4) show that the FeO and TiO_2 abundances associated with the dark rays west of Dionysius generally decrease as a function of distance from the parent crater. This suggests that lesser amounts of mare basalts are present in the distal portions of the dark rays. The five-point spectra obtained for the dark rays west of Dionysius also indicate that smaller amounts of basaltic debris are present at greater distances from the crater. Spectra were collected for the proximal and distal portions of three dark rays west of Dionysius (Figure 3 and Table 2). For each ray, the spectrum obtained for the more distal area

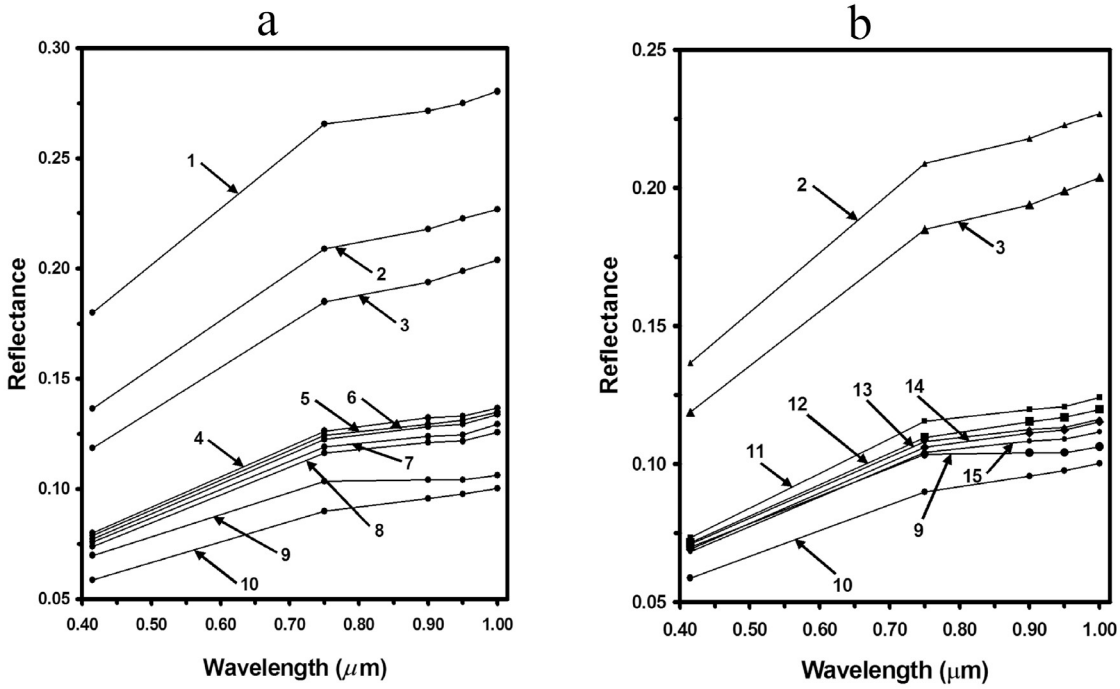

Figure 5. (a) Five-point Clementine UV-VIS spectra obtained for features in the Dionysius region. The areas for which these spectra, as well as those shown in Figure 5b, were collected are shown in Figure 3 and described in Table 2. (b) Additional five-point Clementine UV-VIS spectra for features in the Dionysius region.

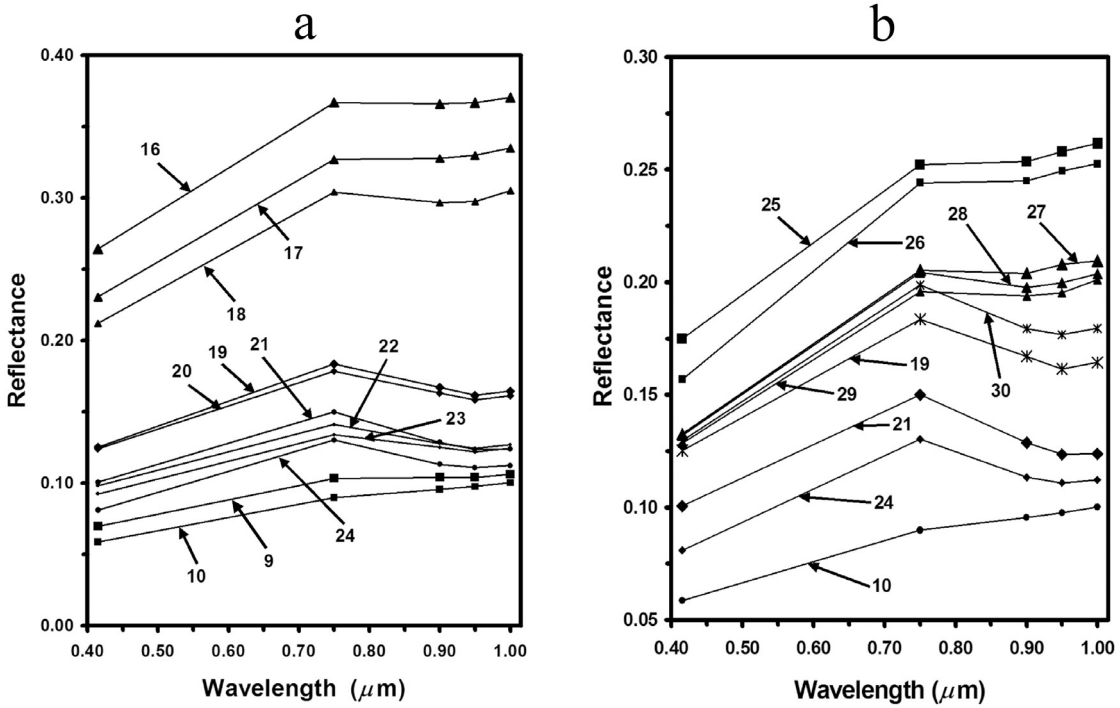

Figure 6. (a) Five-point Clementine UV-VIS spectra collected for features in the Dionysius region. The areas for which these spectra, as well as those shown in Figure 6b, were obtained are shown in Figures 3 and 7b and described in Table 2. (b) Additional Clementine UV-VIS spectra for features in the Dionysius region.

exhibits higher reflectance values than the spectrum collected for the proximal ray segment (Figure 5). The decrease in mare abundances in a given ray as a function of distance from Dionysius may be caused by one or more of the following: (1) lesser amounts of primary ejecta being transported to greater distances, (2) changes in the proportions of highland and mare material in the primary ejecta deposited along the various rays, or (3) the incorporation of increasing amounts of local, nonmare material into dark ray deposits by secondary cratering processes at greater distances from the parent crater [e.g., *Oberbeck*, 1975; *Oberbeck et al.*, 1974, 1975a, 1975b; *Pieters et al.*, 1985].

[15] Well-developed rays also occur east of Dionysius. While *Morris and Wilhelms* [1967] mapped only bright rays east of the crater, they noted that these light rays may have dark central stripes. *Schultz* [1976] described dark, filamentary rays east of Dionysius, and *Smalley* [1965] noted that several dark rays extend east over the surface of Mare Tranquillitatis. Figures 3 and 7b clearly show that both dark and bright rays occur east of Dionysius crater.

[16] In order to investigate the composition of the dark rays east of Dionysius, five-point spectra were extracted for four dark ray segments. The areas for which these spectra were obtained are shown in Figure 3 and described in Table 2. These spectra are numbered 12–15 in Figure 5b. The eastern dark ray spectra exhibit "1 μm" absorption features and band shapes that indicate the presence of mafic assemblages dominated by high-Ca clinopyroxene. The four spectra obtained for these eastern dark rays are even more similar to the spectra collected for the relatively young impact craters in Mare Tranquillitatis (e.g., 9 in Figure 5b) than are those acquired for the dark rays west of Dionysius (Figure 5a). This suggests that even smaller amounts of highland material are present in the dark rays east of the crater.

[17] The chemical values exhibited by the eastern dark rays (Figure 4 and Table 1) also indicate that less highland debris is present. The average FeO and TiO_2 values for the dark ray segments listed in Table 1 range between 15.8 wt % and 16.5 wt % FeO and from 7.0 wt % to 8.0 wt % TiO_2. These values are higher than those determined for the darkest portions of the rays west of Dionysius (Table 1).

[18] The available spectral and chemical data indicate that the dark rays east of Dionysius contain higher abundances of mare basalt than the dark rays located to the west of the crater. This may be due to the fact that the primary ejecta deposited east of Dionysius was emplaced on a mare surface. Hence the local debris that was mixed into the dark ray deposits by secondary cratering processes was mare material. As discussed in the following section, mare material may have been more abundant in the eastern portion of the Dionysius preimpact target site. If so, primary ejecta deposited east of the crater would contain a higher percentage of mare basalt.

3.1.2. Bright Rays

[19] The Clementine FeO and TiO_2 maps (Figure 4 and Table 1) were utilized to investigate the compositions of the bright rays east of Dionysius crater. The bright rays exhibit lower FeO and TiO_2 values than the adjacent dark material. The average FeO and TiO_2 values for three areas (J, K, and L in Figure 4a) along a bright ray directly east of the crater range between 10.3 wt % and 12.8 wt % FeO and 3.4 wt %

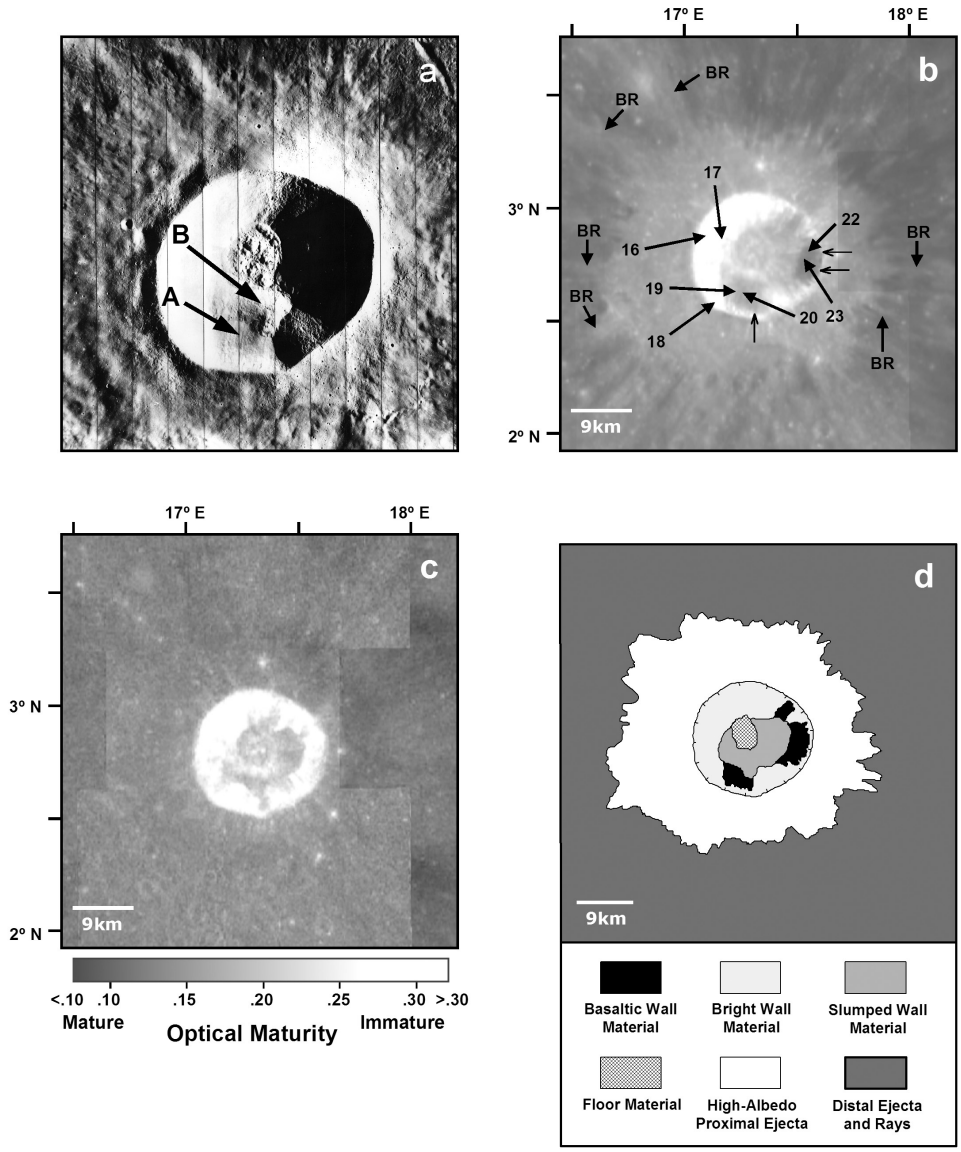

Figure 7. (a) Portion of Lunar Orbiter V frame 83-M showing details on the interior of Dionysius crater. A indicates dark material on the southern crater wall. B indicates slumped wall material. Dionysius is 18 km in diameter. North is toward the top. (b) Clementine 750 nm image mosaic of Dionysius crater. The numbered arrows show the locations where the spectra shown in Figure 6 were collected (see Table 2). The small arrows indicate the top of dark, basaltic material on the south and east walls of the crater. Note that the dark material does not extend completely to the top of either wall. BRs indicate the locations of selected bright rays. (c) Optical maturity parameter image produced for the area shown in Figure 7b. Brighter tones indicate lower maturity (fresher material). (d) Geologic sketch map of that portion of the Dionysius region shown in Figure 7b.

and 5.5 wt % TiO_2. These light rays contain a large, though variable component of highland material. The OMAT values obtained for the east bright ray segments indicate that they are not fully mature (Table 1).

[20] High-albedo rays also occur west of Dionysius (Figures 3 and 7b). These rays exhibit FeO and TiO_2 values that are lower than the adjacent dark ray surfaces (Figure 4) and OMAT values that indicate that bright ray surfaces are not fully mature (Figure 7c). The lower FeO and TiO_2 values indicate that these bright rays contain greater amounts of highland materials than the adjacent dark rays. These high-albedo rays, as well as those east of Dionysius, are bright largely because of the contrast in albedo between ray material containing highland-rich ejecta and the adjacent mare-rich surfaces. Since the OMAT values indicate that the high-albedo rays are not fully mature, immaturity plays a minor role in producing the brightness of these rays. Rays that are bright because of compositional contrast with the surrounding terrain and the presence of immature material have been defined as ''combination'' rays by *Hawke et al.* [2004]. With increasing age, the bright rays of Dionysius will become fainter as the surfaces mature. Eventually, these

Table 2. Description of the Areas for Which the Spectra Shown in Figures 5 and 6 Were Obtained

Spectrum Number	Description of Area
1	bright ejecta north of Dionysius
2	bright ejecta NW of Dionysius
3	bright ejecta SW of Dionysius
4	SW dark ray (distal)
5	NW dark ray (distal)
6	west dark ray (distal)
7	SW dark ray (proximal)
8	west dark ray (proximal)
9	Mare Tranquillitatis crater
10	mature Mare Tranquillitatis surface
11	NW dark ray (proximal)
12	SE dark ray (proximal)
13	SE dark ray (distal) 1
14	SE dark ray (distal) 2
15	east dark ray
16	NW wall of Dionysius 1
17	NW wall of Dionysius 2
18	SW wall of Dionysius
19	south wall of Dionysius 1
20	south wall of Dionysius 2
21	fresh Mare Tranquillitatis crater 1
22	east wall of Dionysius 1
23	east wall of Dionysius 2
24	fresh Mare Tranquillitatis crater 2
25	south wall of Ariadaeus crater
26	west wall of Cayley crater
27	east wall of Cayley crater
28	Cayley plains crater 1
29	Ariadaeus B rim
30	Cayley plains crater 2

"combination" rays will evolve into compositional rays when their surfaces reach complete optical maturity.

3.2. Dionysius Crater Interior

[21] Since mafic debris was ejected during the Dionysius impact event, we have attempted to determine the origin of this material. Did Dionysius excavate surface basalt flows, buried mare basalts (cryptomare), or an intrusive igneous complex of basaltic composition? The surface of the proximal ejecta deposit surrounding Dionysius should be dominated by material derived from the greatest depth within the preimpact target site [e.g., *Shoemaker*, 1963; *Stöffler et al.*, 1975]. As discussed above, the high-albedo proximal ejecta (Figures 4 and 7d) is relatively low in FeO and TiO_2, and is dominated by anorthositic norite. Hence it appears unlikely that the basaltic material in the dark rays was excavated from a deep mafic intrusion. The material present in distal ejecta deposits such as the dark rays should have been derived from a much shallower surface or near-surface layer. Additional evidence for a shallow origin is provided by remote sensing data obtained for the interior of Dionysius crater.

[22] Lunar Obiter photographs (Figures 2 and 7a) and Clementine images (Figures 7b and 7c) were used to produce the geologic sketch map of Dionysius shown in Figure 7d. Dionysius has a relatively small, complex floor which exhibits several small hills (Figure 7a). These hills are surrounded by ropy material that is probably rich in impact melt. Portions of the floor have been covered by material slumped from the crater wall (see arrow B in Figure 7a). Dark material with relatively high FeO and TiO_2 abundances occurs on the northeastern, eastern, and southern portions of the crater wall (Figures 4 and 7). The optical maturity parameter image (Figure 7c) shows that the dark wall material is very immature, which suggests recent downslope movement of material. The FeO values for the darkest portion of the east wall deposit range between 15.0 wt % and 17.0 wt % and suggest a basaltic composition. The small arrows in Figure 7b indicate the highest exposures of dark material on various portions of the crater wall. A crucial observation is that the dark material does not extend completely to the top of the wall. The dark debris appears to have been derived from an iron-rich layer very high on the crater wall.

[23] In order to further investigate the composition of the dark wall material, five-point spectra were extracted for both bright and dark portions of the crater wall. The areas for which these spectra were obtained are shown in Figure 7b and described in Table 2. These seven spectra are presented in Figure 6a. The spectra for two dark areas (22 and 23) on the east wall of Dionysius are very similar to those obtained for two very immature craters in Mare Tranquillitatis (21 and 24 in Figure 6a) which expose fresh mare basalts. These east wall spectra exhibit "1 μm" absorption features and the spectral parameters indicate mafic assemblages dominated by high-Ca clinopyroxene. The areas for which the east wall spectra were obtained are composed largely of mare basalts. The spectra for two dark areas (19 and 20) on the south wall similarly indicate that these areas also contain abundant mare material. However, more highland material is present in the dark material of the south wall than that on the east wall, as evidenced by the higher reflectance values of the south wall spectra.

[24] In summary, the currently available spectral and geochemical data indicate that the dark material exposed on the wall of Dionysius crater is dominated by mare basalt.

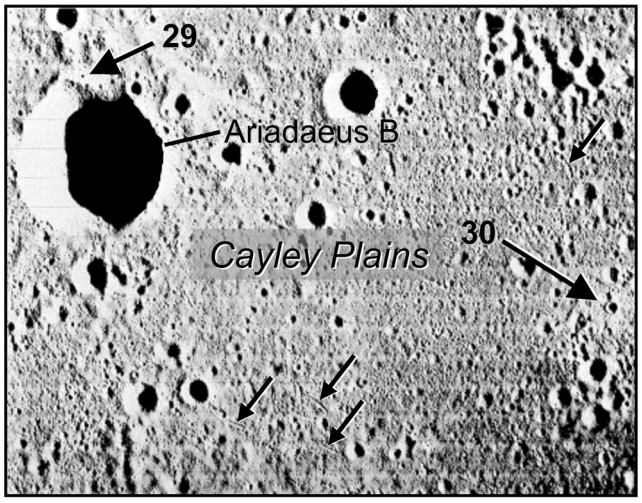

Figure 8. Portion of Lunar Orbiter frame 61-M showing the Cayley plains northwest of Dionysius crater. Ariadaeus B is 8 km in diameter. North is toward the top. The numbered arrows show the locations where two spectra (29 and 30) shown in Figure 6b were obtained (see Table 2). The arrow labeled 30 points to an extremely fresh crater that is 650 m in diameter. The unnumbered black arrows indicate Dionysius secondary crater chains.

The source of the basaltic debris was an iron-rich layer visible very near the top of the crater wall. This layer probably represents a mare deposit that was present at the surface of the preimpact target site. Since the dark material occurs on the northeastern, eastern, and southern segments of the crater wall, the mare deposit may have been thicker and more extensive in the eastern and southern portions of the target site. The spectral characteristics of this mare unit suggest that it may be a westward extension of the basalt flows in Mare Tranquillitatis.

3.3. Cryptomare Deposits

[25] Major expanses of light plains deposits occur in the Dionysius region (Figure 2). Since several workers have suggested that cryptomare deposits are associated with Cayley plains in the region [e.g., *Staid et al.*, 1996], we used Clementine multispectral images and a variety of spacecraft photography to search for buried mare basalts. Criteria for the identification of cryptomaria have been presented by *Schultz and Spudis* [1979], *Hawke and Spudis* [1980], and *Antonenko et al.* [1995]. Chief among these is the presence of dark-haloed impact craters. A few dark-haloed craters (DHCs) of impact origin were identified in the region. One of these DHCs is indicated in Figure 3. All are located on mare surfaces near the highland-mare boundary. Apparently, these dark haloes were formed by the excavation and emplacement of pure mare basalts on mare surfaces that have been contaminated by nonmare debris from the nearby highlands [e.g., *Li and Mustard*, 2000b, 2003]. No well-developed dark-haloed impact craters were identified on Cayley plains in the Dionysius region (Figure 3). However, DHCs on Imbrium ejecta deposits have been located northwest of the study region. Two examples are indicated in Figure 1.

[26] Spectral and chemical data were obtained for Cayley, De Morgan, and Ariadaeus B craters (Figures 2, 3, and 8). These moderate-sized craters (8–14 km in diameter) should have penetrated the Cayley plains and exposed any subjacent mare deposits. Two spectra (26 and 27) for the interior of Cayley crater and one spectrum (29) for the rim of Ariadaeus B crater are shown in Figure 6b. These spectra exhibit "1 μm" absorption features, and the band shapes indicate mafic assemblages dominated by low-Ca pyroxene. These spectra are similar to the spectrum (25) obtained for the highland material on the south wall of Ariadaeus crater (Figure 6b). No spectral evidence for buried mare basalts was provided by these craters. In addition, the FeO and TiO_2 data (Figure 4) indicated that Cayley, De Morgan, and Ariadaeus B craters did not excavate cryptomare material.

[27] *Staid and Pieters* [1998] presented Clementine UV-VIS spectra for small (<2 km) impact craters located on Cayley plains west and northwest of Dionysius. They noted that the shape and strength of the "1 μm" absorption features in the spectra obtained for the small Cayley plains craters are consistent with a noritic composition, rather than a basaltic or gabbroic composition. We also extracted five-point spectra for small, fresh craters on the Cayley Formation from a Clementine UV-VIS image cube. A typical spectrum (28) is shown in Figure 6b. This spectrum has a "1 μm" absorption band centered near 0.90 μm, which indicates a mafic assemblage dominated by low-Ca pyroxene. A noritic composition is demonstrated for the area for which the spectrum was obtained. With one exception, our results indicate that small craters in the Cayley plains west and northwest of Dionysius excavated noritic material and confirm the findings of *Staid and Pieters* [1998].

[28] The exception is a small (diameter = 650 m) impact crater located on light plains northeast of Cayley crater (30 in Figure 3 and Figure 8). The spectrum (30) obtained for this extremely fresh crater is shown in Figure 6b. The spectral parameters exhibited by this fresh crater suggest the presence of both low- and high-Ca pyroxene. Note that the spectrum (30) of this small crater is very similar to the spectrum (19) extracted for a dark area on the south wall of Dionysius that was interpreted to represent a mixture of mare and highland debris (Figure 6b). Figure 4a shows that this small crater (R in Figure 4a and Table 1) exhibits slightly enhanced FeO values (13.4 wt %) relative to the surrounding Cayley plains. While the crater is on the trace of a Dionysius dark ray (Figure 3), the mafic ray material is not responsible for the relatively high FeO values associated with this small impact structure. The crater, which exhibits an OMAT value of 0.329, is extremely immature. This very young crater formed after the Dionysius impact event and would have penetrated the thin Dionysius dark ray deposit and exposed subjacent material. Additional evidence that the enhanced FeO values associated with this small crater are not related to Dionysius ray material is provided by the TiO_2 map shown in Figure 4b. The small crater exhibits an average TiO_2 concentration of 1.6 wt % (R in Table 1). The dark rays of Dionysius have much higher TiO_2 values (Figure 4b and Table 1). The small crater may have exposed a clinopyroxene-rich facies of the Cayley Formation, or it may have penetrated the light plains deposit and excavated at least some buried mare material.

[29] There is additional evidence that some portions of the Cayley Formation in the Dionysius region are more mafic than others. For example, the Cayley plains material exposed in portions of the walls of Rima Ariadaeus exhibits enhanced FeO values (13–15 wt %, Figure 4a). An area of the Cayley Formation, near Rims Ariadaeus, with a relatively low albedo is labeled Dark Cayley in Figure 3. The Dark Cayley Plains (S in Figure 4a and Table 1) have an average FeO value of 13.2 wt % which is somewhat higher than the range of values (9–10 wt %) exhibited by typical Cayley plains in the region. The Dark Cayley FeO value (13.2 wt %) is almost identical to that determined for the small crater discussed above (13.4 wt %). However, the relatively high TiO_2 abundances (~3.4 wt %) associated with the Dark Cayley Plains suggests that they are not composed of the same lithology as that exposed by the small crater since this material has an average TiO_2 concentration of 1.6 wt %.

[30] While the Dark Cayley may be a mafic facies of the Cayley Formation, other origins are possible. The FeO and TiO_2 values associated with the Dark Cayley are similar to those exhibited by the distal portions of several dark rays (Figure 4 and Table 1). Hence the low albedo and enhanced FeO and TiO_2 values of the Dark Cayley could be the result of contamination of light plains deposits by distal, mafic dark ray material ejected from Dionysius crater. Alternately, though less likely, the Dark Cayley may have been formed by the emplacement of a thin layer of dark mantle material of pyroclastic origin. A previously unidentified dark mantle

deposit is located in the highlands just northwest of Ariadaeus E crater and is labeled DMD in Figure 3.

4. Summary and Conclusions

[31] 1. Spectra obtained for the high-albedo proximal ejecta (Figure 7d) of Dionysius crater exhibit high reflectance values and have absorption bands centered near 0.90 μm, which suggests a mafic assemblage dominated by low-Ca pyroxene. Both the spectral and chemical data indicate that these proximal ejecta deposits are composed largely of anorthositic norites. In contrast, the spectra extracted for young craters in Mare Tranquillitatis have deep "1 μm" absorption features and the band shapes indicate mafic assemblages dominated by high-Ca clinopyroxene.

[32] 2. Well-developed dark rays occur in the highlands west of Dionysius crater (Figure 3). The spectra obtained for dark ray segments west of Dionysius are very similar to those collected for craters in Mare Tranquillitatis and have "1 μm" absorption bands that are centered near 0.95 μm, which indicate the dominance of high-Ca pyroxene. The portions of the dark rays for which spectral and chemical data were obtained are composed of mare debris contaminated with minor amounts of highland material. Both the five-point spectra and the optical maturity parameter values indicate that the dark rays are dominated by mare basalts, not impact melts.

[33] 3. The dark rays west of Dionysius generally become brighter at greater distances from the parent crater until they disappear (Figure 1 and 3). Both the chemical and spectral data for these rays indicate that lesser amounts of mare material are present in the distal portions of the dark rays. The decrease in mare abundances in a given ray as a function of distance from Dionysius may be caused by one or more of the following: a) lesser amounts of primary ejecta being transported to greater distances, b) changes in the proportions of mare and highland material in the primary ejecta deposited along the various rays, or c) the incorporation of increasing amounts of local, nonmare debris into dark ray deposits by secondary cratering processes at greater distances from the parent crater.

[34] 4. Dark rays also extend east of Dionysius over the surface of Mare Tranquillitatis (Figure 3). The available spectral and chemical data indicate that the dark rays east of Dionysius contain higher abundances of mare basalt than the dark rays located west of the crater. This is probably due to the fact that the primary ejecta deposited east of the crater was emplaced on a mare surface. As a result, the local debris that was mixed into the dark ray deposits by secondary cratering processes was mare basalt instead of low-iron highland material. In addition, the geologic mapping of Dionysius (Figure 7d) has revealed that mare basalts were more abundant in the eastern portion of the Dionysius preimpact target site. Hence the primary ejecta deposited east of the crater would contain a higher percentage of mare basalt.

[35] 5. The high-albedo rays associated with Dionysius (Figures 3 and 7b) exhibit FeO and TiO_2 values that are lower than those of the adjacent dark ray surfaces (Figure 4) and optical maturity parameter values that indicate that bright ray surfaces are not fully mature (Table 1). These high-albedo rays are bright largely because of the contrast in albedo between ray material containing highlands-rich ejecta and the adjacent mare-rich surfaces. Since the OMAT values indicate that the high-albedo rays have almost reached full optical maturity, immaturity plays a minor role in producing the brightness of these rays.

[36] 6. The material present in distal ejecta deposits such as the dark rays should have been derived from relatively shallow depths. Support for a shallow origin was provided by remote sensing data obtained for the interior of Dionysius crater. Dark material with relatively high FeO and TiO_2 abundances occurs on the northeastern, eastern, and southern portions of the crater wall (Figures 4 and 7). The currently available spectral and geochemical data indicate that the dark material exposed on the wall of Dionysius is dominated by mare basalt. The source of this basaltic debris was a dark, iron-rich layer visible near the top of the crater wall. This layer represents a mare unit that was present at the surface of the preimpact target site. Our mapping suggests that the mare deposit may have been thicker and more extensive in the eastern and southern portions of the target site. The compositional and spectral characteristics of this mare unit indicate that it may be a westward extension of the basalt flows in Mare Tranquillitatis.

[37] 7. Major expanses of Cayley plains occur in the Dionysius region (Figure 2). Moderate-sized craters (8–14 km in diameter) such as Cayley, De Morgan, and Ariadaeus B should have penetrated the light plains deposits and exposed any subjacent mare deposits. Clementine spectral and chemical data indicate that these craters did not excavate cryptomare material. With one exception, our results indicate that smaller craters on the Cayley Formation west and northwest of Dionysius excavated noritic material, not buried mare basalts. The exception is a small crater located on light plains northeast of Cayley crater which may have exposed a clinopyroxene-rich facies of Cayley Formation, or it may have penetrated the light plains deposit and excavated at least some buried mare basalt.

[38] **Acknowledgments.** The authors would like to thank Charles Wood and Rebecca Ghent for very constructive reviews of the paper. This research was supported by the NASA Planetary Geology and Geophysics Program. This is HIGP publication 1426 and SOEST contribution 6728.

References

Antonenko, I., J. W. Head, J. F. Mustard, and B. R. Hawke (1995), Criteria for the detection of lunar cryptomaria, *Earth Moon Planets*, *69*, 141–172.

Bell, J. F., and B. R. Hawke (1984), Lunar dark-haloed impact craters: Origin and implications for early mare volcanism, *J. Geophys. Res.*, *89*, 6899–6910.

Blewett, D. T., and B. R. Hawke (2001), Remote sensing and geological studies of the Hadley-Apennine region of the Moon, *Meteorit. Planet. Sci.*, *36*, 701–730.

Blewett, D. T., B. R. Hawke, P. G. Lucey, G. J. Taylor, R. Jaumann, and P. D. Spudis (1995), Remote sensing and geologic studies of the Schiller-Schickard region of the Moon, *J. Geophys. Res.*, *100*, 16,959–16,977.

Blewett, D. T., P. G. Lucey, B. R. Hawke, and B. L. Jolliff (1997), Clementine images of the sample-return stations: Refinement of FeO and TiO_2 mapping techniques, *J. Geophys. Res.*, *102*, 16,319–16,325.

Eliason, E. M., et al. (1999), Digital processing for a global multispectral map of the Moon from the Clementine UV-VIS imaging instrument, *Lunar Planet. Sci.* [CD-ROM], *XXX*, Abstract 1933.

Giguere, T. A., B. R. Hawke, D. T. Blewett, D. B. J. Bussey, P. G. Lucey, G. A. Smith, P. D. Spudis, and G. J. Taylor (2003), Remote sensing studies of the Lomonosov-Fleming region of the Moon, *J. Geophys. Res.*, *108*(E11), 5118, doi:10.1029/2003JE002069.

Hapke, B. (2001), Space weathering from Mercury to the asteroid belt, *J. Geophys., Res.*, *106*, 10,039–10,073.

Hawke, B. R., and J. F. Bell (1981), Remote sensing studies of lunar dark-halo impact craters: Preliminary results and implications for early volcanism, *Proc. Lunar Planet. Sci. Conf.*, *12th*, 665–678.

Hawke, B. R., and P. D. Spudis (1980), Geochemical anomalies on the eastern limb and farside of the moon, in *Proceeding of Conference on Lunar Highlands Crust*, edited by J. J. Papike and R. B. Merrill, pp. 467–481, Elsevier, New York.

Hawke, B. R., D. MacLaskey, and T. B. McCord (1979), Multispectral imaging of lunar crater deposits, in *Papers Presented to the Conference on the Lunar Highlands Crust*, pp. 50–52, Lunar and Planet. Inst., Houston, Tex.

Hawke, B. R., P. D. Spudis, and P. E. Clark (1985), The origin of selected lunar geochemical anomalies: Implications for early volcanism and the formation of light plains, *Earth Moon Planets*, *32*, 257–273.

Hawke, B. R., T. A. Giguere, D. T. Blewett, P. G. Lucey, G. A. Smith, G. J. Taylor, and P. D. Spudis (2002), Igneous activity in the southern highlands of the Moon, *J. Geophys. Res.*, *107*(E12), 5122, doi:10.1029/2000JE001494.

Hawke, B. R., D. T. Blewett, P. G. Lucey, G. A. Smith, J. F. Bell III, B. A. Campbell, and M. S. Robinson (2004), The origin of lunar crater rays, *Icarus*, *170*, 1–16.

Isbell, C. E., et al. (1999), Clementine: A multispectral digital image archive of the Moon, *Lunar Planet. Sci.* [CD-ROM], *XXX*, Abstract 1812.

Jolliff, B. L. (1999), UVVIS multispectral data and the Apollo17 landing site: What can we tell and how well?, *J. Geophys. Res.*, *104*, 14,123–14,148.

Li, L., and J. F. Mustard (2000a), The compositional gradients and lateral transport by dark-halo and dark-ray craters, *Lunar Planet. Sci.* [CD-ROM], *XXXI*, Abstract 2007.

Li, L., and J. F. Mustard (2000b), Compositional gradients across mare-highland contacts: The importance of lateral mixing and geological implications, *J. Geophys. Res.*, *105*, 20,431–20,450.

Li, L., and J. F. Mustard (2003), Highland contamination in lunar mare soils: Improved mapping with multiple end-member spectral mixture analysis (MESMA), *J. Geophys. Res.*, *108*(E6), 5053, doi:10.1029/2002JE001917.

Lucey, P. G., G. J. Taylor, and E. Malaret (1995), Abundance and distribution of iron on the Moon, *Science*, *268*, 1150–1153.

Lucey, P. G., D. T. Blewett, and B. R. Hawke (1998), Mapping the FeO and TiO_2 content of the lunar surface with multispectral imagery, *J. Geophys. Res.*, *103*, 3679–3699.

Lucey, P. G., D. T. Blewett, and B. L. Jolliff (2000a), Lunar iron and titanium abundance algorithms based on final processing of Clementine UV-VIS data, *J. Geophys. Res.*, *105*, 20,297–20,305.

Lucey, P. G., D. T. Blewett, G. J. Taylor, and B. R. Hawke (2000b), Imaging of lunar surface maturity, *J. Geophys. Res.*, *105*, 20,377–20,386.

Morris, E. C., and D. E. Wilhelms (1967), Geologic map of the Julius Caesar quadrangle of the Moon, *U.S. Geol. Surv. Misc. Invest. Ser. Map*, *I-510*.

Nozette, S., et al. (1994), The Clementine mission to the Moon: Scientific overview, *Science*, *266*, 1835–1839.

Oberbeck, V. R. (1975), The role of ballistic erosion and sedimentation in lunar stratigraphy, *Rev. Geophys.*, *13*(2), 337–362.

Oberbeck, V. R., R. H. Morrison, F. Hörz, W. L. Quaide, and D. E. Gault (1974), Smooth plains and continuous deposits of craters and basins, *Proc. Lunar Sci. Conf.*, *5th*, 111–136.

Oberbeck, V. R., F. Hörz, R. H. Morrison, W. L. Quaide, and D. E. Gault (1975a), On the origin of the lunar smooth-plains, *Moon*, *12*, 19–54.

Oberbeck, V. R., R. H. Morrison, and F. Hörz (1975b), Transport and emplacement of crater and basin deposits, *Moon*, *13*, 9–26.

Pieters, C. M., J. B. Adams, P. J. Mouginis-Mark, S. H. Zisk, M. O. Smith, J. W. Head, and T. B. McCord (1985), The nature of crater rays: The Copernicus example, *J. Geophys. Res.*, *90*, 12,393–12,413.

Pieters, C. M., J. W. Head, L. Gaddis, B. Jolliff, and M. Duke (2001), Rock types of South Pole-Aitken basin and extent of basaltic volcanism, *J. Geophys. Res.*, *106*, 28,001–28,022.

Robinson, M. S., A. S. McEwen, E. Eliason, E. M. Lee, E. Malaret, and P. G. Lucey (1999), Clementine UV-VIS global mosaic: A new tool for understanding the lunar crust, *Lunar Planet. Sci.* [CD-ROM], *XXX*, Abstract 1931.

Schultz, P. H. (1976), *Moon Morphology*, Univ. of Tex. Press, Austin.

Schultz, P. H., and P. D. Spudis (1979), Evidence for ancient mare volcanism, *Proc. Lunar Planet. Sci. Conf.*, *10th*, 2899–2918.

Shoemaker, E. M. (1963), Impact mechanics at Meteor Crater, Arizona, in *The Moon, Meteorites, and Comets*, edited by B. M. Middlehurst and G. P. Kuiper, pp. 301–336, Univ. of Chicago Press, Chicago, Ill.

Smalley, V. G. (1965), The lunar crater Dionysius, *Icarus*, *4*, 433–436.

Staid, M. I., and C. M. Pieters (1998), A re-evaluation of lunar basalt types through spectral analysis of fresh mare craters, *Lunar Planet. Sci.* [CD-ROM], *XXIX*, Abstract 1853.

Staid, M. I., C. M. Pieters, and J. W. Head (1996), Mare Tranquillitatis: Basalt emplacement history and relation to lunar samples, *J. Geophys. Res.*, *101*, 23,213–23,228.

Stöffler, D., D. E. Gault, J. Wedekind, and G. Polkowski (1975), Experimental hypervelocity impact into quartz sand: Distribution and shock metamorphism of ejecta, *J. Geophys. Res.*, *80*, 4062–4077.

Thomson, B. J., P. D. Spudis, and D. B. J. Bussey (1998), Impact craters as probes of the lunar crust, *Lunar Planet. Sci.* [CD-ROM], *XXIX*, Abstract 1820.

Tompkins, S., and C. M. Pieters (1999), Mineralogy of the lunar crust: Results from Clementine, *Meteorit. Planet. Sci.*, *34*, 25–41.

D. T. Blewett, NovaSol, 733 Bishop Street, 28th Floor, Honolulu, HI 96843, USA.

L. R. Gaddis, U.S. Geological Survey, 2255 North Gemini Drive, Flagstaff, AZ 86001, USA.

T. A. Giguere, J. J. Gillis-Davis, B. R. Hawke, P. G. Lucey, G. A. Smith, and G. J. Taylor, Hawaii Institute of Geophysics and Planetology, University of Hawaii at Manoa, 2525 Correa Road, Honolulu, HI 96822, USA. (tagiguer@ingr.com)

P. D. Spudis, Johns Hopkins University Applied Physics Laboratory, 11100 Johns Hopkins Road, Laurel, MD 20723, USA.